DOI: 10.1143/JJAP.51.01AH01

Applications of Carbon Nanotubes Grown by Chemical Vapor Deposition

John Robertson, Guofang Zhong, C. Santiago Esconjauregui, Bernhard C. Bayer,
Can Zhang, Martin Fouquet, and Stephan Hofmann

Engineering Department, University of Cambridge, Cambridge CB2 1PZ, U.K.

Received April 23, 2011; accepted September 23, 2011; published online January 20, 2012

The requirements for using carbon nanotubes as vias and interconnects are described. The growth of high density forests of vertically-aligned carbon nanotubes for interconnect applications by chemical vapor deposition is described. Densities up to 1.4 x 10^{13} cm^{-2} have been achieved by maintaining a small nanotube diameter. The process integration devices is reviewed. © 2012 The Japan Society of Applied Physics

1. Introduction

Carbon nanotubes (CNTs) have many potential applications due to their unique electronic, thermal and structural properties.[1–4] The continued scaling of semiconductor device dimensions in integrated circuits has led to the replacement of many of the traditional materials. Copper has replaced Al as the metal in interconnects, and high dielectric constant oxides such as HfO_2 have replaced SiO_2 as the gate insulator in the field effect transistors. Interconnects are the metal wires that connect transistors in the integrated circuit, and are both vertical and horizontally oriented (Fig. 1).

In the near future, the current density carried by interconnects is likely to exceed that which can be carried by copper, due to its electromigration limit of about 6×10^6 A/cm^2 (Fig. 2).[5] CNTs or graphene are the only materials that can carry a higher current density, as they are able to carry up to 10^9 A/cm^2 before failure,[2–4] due to their strong covalent bonding. A second reason to use CNTs is that their high thermal conductivity might help dissipate heat in the integrated circuit. A third reason is that the large aspect ratio of CNTs might be helpful for making interconnects that have a high aspect ratio, such as through-silicon vias. Finally, CNTs would not require liners to provide diffusion barriers. These advantages have led to considerable effort to develop CNTs for interconnect applications.[6–29]

Despite these advantages, there have been considerable problems. There are two main difficulties. Firstly, in any economic manufacturing scheme, the CNTs must be grown in place in the via hole or interconnect structure; they cannot be grown elsewhere and placed there. But the standard growth processes are rather incompatible with Si technology. Secondly, interconnects require CNTs of extremely high area density. This arises because CNTs are one dimensional conductors, so that their resistance is the sum of the quantum of conductance per channel R_q plus a resistance per unit length, r. The CNT interconnect should have a resistance below that of the copper equivalent to be useful. This requires us to parallel many CNTs to lower the overall resistance,[25]

$$R = \frac{R_q + r \cdot l}{n},$$

where n is the number of nanotube conducting channels in parallel. Figure 3 shows that it is necessary to increase n to of order 10^{14} cm^{-2} to be below that of Cu for a typical 100 nm high via. This density equals a pitch of ~1.1 nm (on a hexagonal grid). This has recently led to considerable efforts to grow nanotubes in via structures with a maximised area density, guided by the extensive work on the growth of nanotube forests,[30–55] as shown in Fig. 4. Overall, there are four requirements for nanotubes for interconnects, from Robertson *et al.*;[26]

- high density,
- growth on conducting substrates,
- growth at low temperatures (400 °C) compatible with a back end of line (BEOL) process,
- a process integration with the rest of the integrated circuit.

Of these, the emphasis has been on density and low temperature.

Figure 4 compares the area density of various grown nanotube samples to the density of a fully dense, aligned

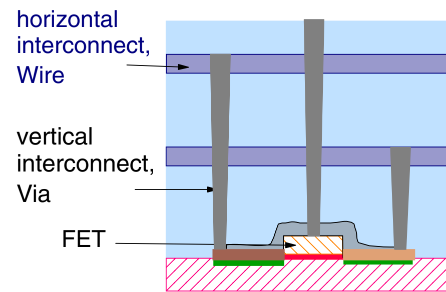

Fig. 1. (Color online) Schematic of horizontal and vertical interconnects in an integrated circuit.

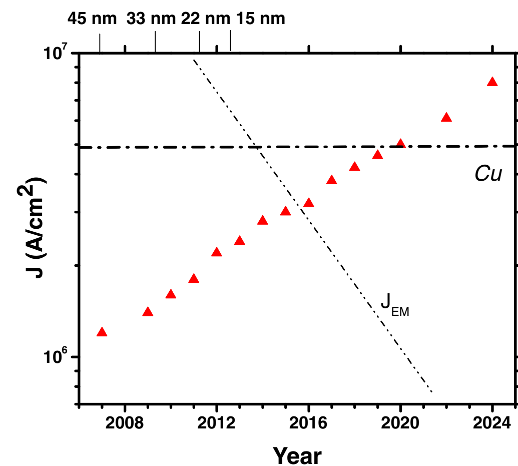

Fig. 2. (Color online) Current density requirements of integrated circuits vs year of development. From Fig. INTC21, ITRS interconnect roadmap.[5] J_{EM} is the electromigration limit of Cu for the target lifetime. The horizontal line is the electromigration limit of macroscopic Cu.

 © 2012 The Japan Society of Applied Physics

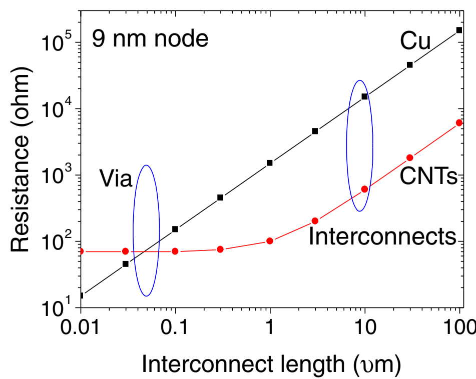

Fig. 3. (Color online) Resistance vs interconnect length of copper and carbon nanotube interconnects, for a nanotube density of 10^{14} cm^{-2}.

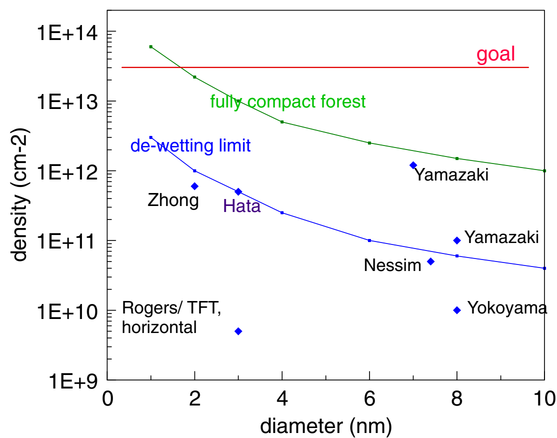

Fig. 4. (Color online) Density of some carbon nanotube forests, compared to the theoretical maximum density and a typical density produced by the catalyst de-wetting method.[17,18,20,24,31,38,56)]

nanotube forest in which the nanotube cylinders are separated by the *c*-axis spacing of graphite of 0.338 nm. This diagram shows that the tall, vertically-aligned forests grown by Hata *et al.*[30,31)] and Zhong *et al.*[38)] do not have particularly high densities. Their area densities of 5×10^{11} cm^{-2} and 9×10^{11} cm^{-2} correspond to only about 5% space filling. On the other hand, work on vias by Nihei *et al.*[12)] tended to produce larger diameter multi-wall nanotubes, and their area density was even lower at 10^{10} to 10^{11} cm^{-2}. Only recently have such groups achieved densities over 10^{11} cm^{-2} and up to 10^{12} cm^{-2}.[17–20,29)] It is interesting that groups such as Rogers *et al.*[56)] growing horizontally-aligned nanotubes for use in thin film transistors achieve densities of about 10 tubes per micrometer, which corresponds to 10^{10} cm^{-2}, much lower than required here.

2. Growth Theory

CNTs for interconnects are grown by catalytic chemical vapor deposition (CVD). The highest density forests tend to grow by the root growth mechanism. The catalyst is active in its high surface area state of a layer of nanoparticles. The standard method of CVD is a three-step process (Fig. 5); first deposit the catalyst as a thin film by evaporation or sputtering, then transform it into nanoparticles by annealing in a particular atmosphere, and then introduce a hydrocarbon gas to allow growth to occur.[26)] It is expected that one nanotube will grow from each catalyst nanoparticle in CVD. In this, CVD growth differs from the high temperature laser-assisted growth in which each catalyst particle tends to nucleate more than one nanotube.[55)] Thus, to achieve the highest tube density, we must maximise the density of catalyst nanoparticles.

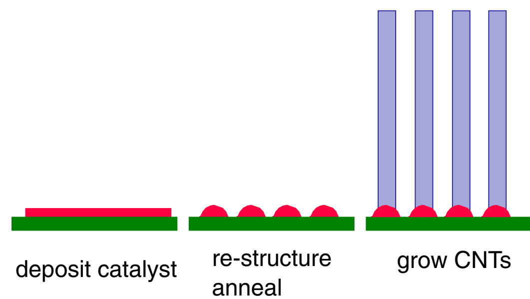

Fig. 5. (Color online) Three step process to produce catalyst, anneal catalyst and grow nanotubes.

Table I. Surface energies of solid metals, metallic compounds and oxides (in J/m^2).

	Experiment	Theory	Refs.
Ni	2.08	2.01	60,61
Co	2.22	2.77	60,61
Fe	2.12, 1.72	2.22	60,61
Mo	2.51	3.45	60,61
Cr	2.00	3.5	60,61
W	2.76	4.0	60,61
Ta	2.49	3.08	60,61
Ti	1.75	2.52	60,61
TiN		1.6, 1.40	64
$ZrSi_2$	0.8–1.2		59
$TiSi_2$	0.8–0.9		59
$CoSi_2$	0.72–0.8	1.65	59
$NiSi_2$		1.13	59
SiO_2	0.043–0.106		63
Al_2O_3	0.062–0.1	0–0.1	62
MgO	0.1		62

Data of Tyson and Miller[60)] are for liquid metals, multiplied by a constant factor of 1.18 to give values for the solid. The values of Vitos *et al.*[61)] were calculated by density functional theory, for the lowest energy face of the crystalline phase.

The transformation of the thin film into nanoparticles is driven by the difference in surface energies of the catalyst metal and the underlying "support" layer.[58)] Consider first typical values of the surface energies (Table I).[58–64)] The elemental metals have surface energies of typically 2 J/m^2, the metallic silicides have surface energies of 1 J/m^2, whereas the insulating oxides are much lower at 0.1 J/m^2.

The process generally uses this annealing method. It is also possible to use a cluster beam to deposit catalyst nanoparticles.[19)] This is produced by condensing gas of metal atoms into nanoparticles using an inert gas stream, particle size separation, and then scanning the beam across the desired area. This process can be employed, however it is much less economic.

The transformation of the thin film catalyst into nanoparticles is driven by the reduction in interfacial energy, see

© 2012 The Japan Society of Applied Physics

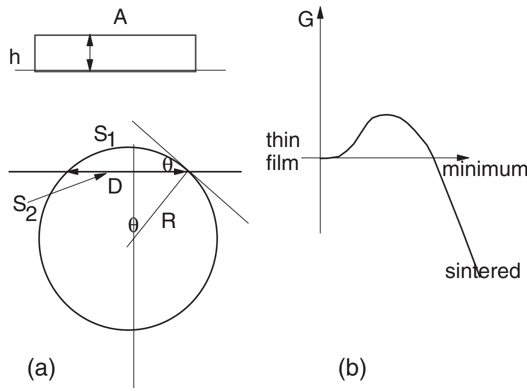

Fig. 6. (a) Geometries of the de-wetting process, and (b) free energies of the de-wetting process.

Figs. 6(a) and 6(b). The surface energy of the catalyst is denoted σ_1, that of the support layer σ_2 and the interfacial energy is σ_{12}. The free energy of a thin film of thickness h of catalyst on a support is given by

$$G_1 = A(\sigma_1 + \sigma_{12}). \tag{1}$$

With reference to the geometries in Fig. 6(a), the free energy of an array of truncated spheroidal particles of diameter D, area density N and contact angle θ is

$$G_2 = (A - NS_2)\sigma_2 + NS_1\sigma_1 + NS_2\sigma_{12}, \tag{2}$$

where

$$S_1 = 2\pi R^2(1 - \cos\theta), \tag{3}$$

$$S_2 = \pi R^2 \sin^2\theta. \tag{4}$$

The contact angle is derived from Young's equation,

$$\sigma_2 = \sigma_{12} + \sigma_1 \cos\theta \tag{5}$$

and the conservation of catalyst volume gives

$$hA = NV_{\text{cat}}, \tag{6}$$

where

$$V_{\text{cat}} = \frac{\pi R^3}{3}(1 - \cos\theta)^2(2 + \cos\theta). \tag{7}$$

De-wetting occurs if [see Fig. 6(b)]

$$G_2 \leq G_1, \tag{8}$$

or, by using eqs. (1), (2), and (7)

$$A(\sigma_2 - \sigma_1 - \sigma_{12}) + N(S_1\sigma_1 - S_2\sigma_2 + S_2\sigma_{12}) < 0. \tag{9}$$

Using eq. (5), this gives

$$-A\sigma_1(1 + \cos\theta) + N\sigma_1(S_1 - S_2\cos\theta) < 0 \tag{10}$$

and σ_1 cancels through. Substituting for A from eq. (6), and using eqs. (3) and (4) gives

$$\frac{R}{3}(1 - \cos\theta)^2(2 + \cos\theta) \geq h[2 - (1 + \cos\theta)\cdot\cos\theta] \tag{11}$$

or

$$R = \frac{3h}{1 - \cos\theta}. \tag{12}$$

Using the particle's projected diameter $D = 2R\sin\theta$, this is

$$D = 6h\left(\frac{1 + \cos\theta}{1 - \cos\theta}\right)^{1/2}, \tag{13}$$

and the particle density is found to be

$$N = \frac{(1 - \cos\theta)}{9\pi h^2(2 + \cos\theta)}, \tag{14}$$

or

$$N = \frac{4(1 + \cos\theta)}{\pi D^2(2 + \cos\theta)}.$$

A typical value for $\theta = 90°$ is $N = 0.6/D^2$. Note that this gives the maximum density possible by the de-wetting method. G_2 can lower itself by sintering (increase of the particle diameter) and this lowers N, as shown in Fig. 6(b).

The key observation is that the maximum N value obtainable by this method is lower than the maximum theoretical density of an array of single wall CNTs (SWNTs) (Fig. 4).

3. Growth of High Density Forests

The best catalysts for growing CNTs are Fe, Co, and Ni. The highest density CNT forests have usually been grown using Fe as catalyst and Al_2O_3 as the support layer,[28,36,38,44] for both single-walled and multiwalled forests. One reason for the good performance of Fe on Al_2O_3 is that there is an interfacial chemical reaction between the Fe and Al_2O_3 which produces an Fe aluminate, as seen by *in-situ* X-ray photoemission spectroscopy (XPS).[50] The interfacial reaction tends to anchor the Fe nanoparticles, and reduce any tendency to sintering. It leads to a narrower distribution of catalyst nanoparticles, of higher density, and thus to a higher density forest. The forest grows by root growth mechanism, and the high density produces the vertical alignment of the forest, by a crowding mechanism.

We have developed two methods to increase the density of the forests. The first method is to reduce the nanotube diameter D, by reducing the initial thickness of the catalyst film. This increases N, as D is proportional to h from eq. (12) and N varies as h^{-2}.

Hasegawa and Noda[55] found that reducing the initial thickness of the Fe film first leads to higher growth, but then causes a loss of yield and limited growth. We analysed the catalyst layer by secondary ion mass spectrometry (SIMS) and Auger. We found that the Fe tends to diffuse into the Al_2O_3, and then build up at the interface between the Si and Al_2O_3 where it is blocked (Fig. 7). Thus, Al_2O_3 is a useful support layer because its surface properties and often higher surface area leads to lower diffusion on the surface. However, the type of Al_2O_3 does affect the forest density as found by Amama.[48] Its porosity can allow the catalyst to diffuse away from the surface, causing a loss of catalyst growth activity. It is necessary to stop this.

We grew the Al_2O_3 by depositing a thin layer of Al by evaporation and then carried out a room temperature plasma oxidisation of the Al to Al_2O_3. The plasma oxidation creates a densified Al_2O_3 with a much reduced Fe diffusion. This allows us to reduce the initial Fe thickness.

The CNTs where grown in a cold wall thermal CVD chamber with a rapid substrate heater, is a hydrogen diluted acetylene gas flow, at a pressure of 15 mbar at 700 °C.

 © 2012 The Japan Society of Applied Physics

Acetylene is the primary growth species for CNTs, as was shown by molecular beam experiments of Eres[65] and mass spectrometry studies of Zhong.[43]

Figure 8 shows high resolution transmission electron microscope (HRTEM; JEOL 4000) and scanning electron microscope (SEM; Philips XL30 SFEG) images of the resulting CNT forest. Due to its higher density, the forest does not grow to millimetres high. The area density is measured in three ways. First, we can count the number of tubes from the SEM images. Second, we can measure the sample's weight gain during growth, measure the diameter and number of walls by TEM, and thereby derive the mass per unit length of the CNT, and from the ratio, this gives the area density. The third way is to use liquid-induced compaction. Applying drops of isopropyl alcohol or ethanol causes the CNT forest to form locally compacted regions. These have previously aroused interest for their patterns by Chakrapani.[66] Futaba *et al.*[31] previously estimated the area density from the ratio of the top area of the compacted forest to the total initial area (Fig. 9). The three methods give consistent results. We find that our growth conditions, the average CNT diameter is 1.1 nm, and the tubes are single walled. The mass density of the as-grown layer is 0.245 to 0.345 g/cm^3, giving an area density of 1.05 to 1.45 × 10^{13} cm^{-2}. The compacted density is typically 0.47 to 0.7 g/cm^3, and the ideal compact density of such tubes is 1.53 g/cm^3. We see that our density of 1.45 × 10^{13} cm^{-2} is about 30 times higher than the typical density in "super-growth" samples, as shown in Fig. 10.

The second method to grow denser forests is to increase the nucleation density for larger diameter nanotubes by a novel catalyst treatment process, as in Esconjauregui.[67] The usual annealing process to convert the initial thin film

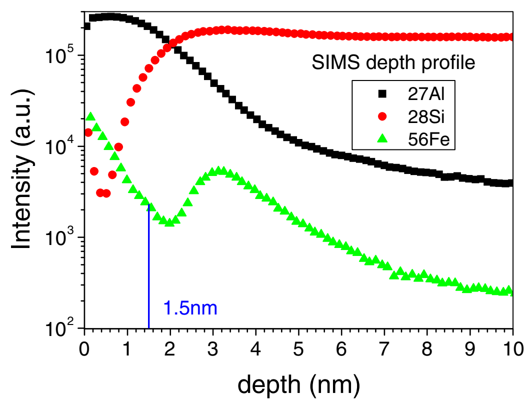

Fig. 7. (Color online) SIMS depth profile of Fe for Fe catalysts on Al_2O_3 support on Si.

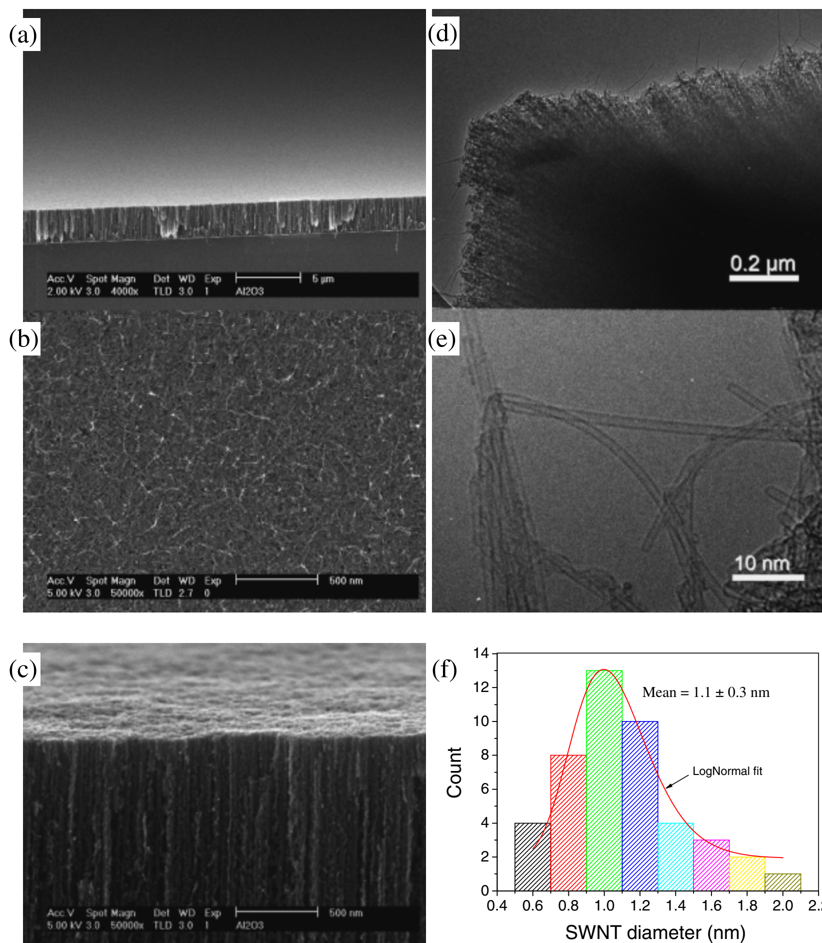

Fig. 8. (Color online) SEM (a) and HRTEM (b) images of ultra-high density (UHD) SWNT forests prepared on 0.5 nm Al/0.4 nm Fe/5 nm Al/Si(100) at 15 mbar, 700 °C, 40 sccm C_2H_2 and 460 sccm H_2 by cold-wall CVD. The 5 nm Al layer had O_2 plasma. (a) A tilt view of the as-grown sample at a low magnification. (b, c) Surface and tilt views at high magnifications. (d, e) Low and high magnification HRTEM images of SWNTs. (f) SWNT diameter distribution from HRTEM images.

© 2012 The Japan Society of Applied Physics

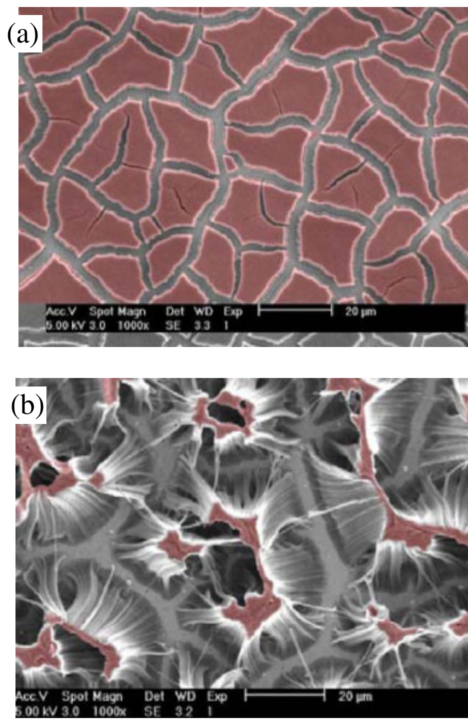

Fig. 9. (Color online) Liquid-induced densification of different SWNT forests by soaking the samples with ethanol and drying in air. (a) The ultra high density SWNT sample grown in 1% C_2H_2, the inset shows the cross-sectional details of the densification effect. (b) A sample of SWNT forests grown for 1% C_2H_2 on 0.5 nm Al/0.7 nm Fe/5 nm Al/Si(100), other conditions same as (a).

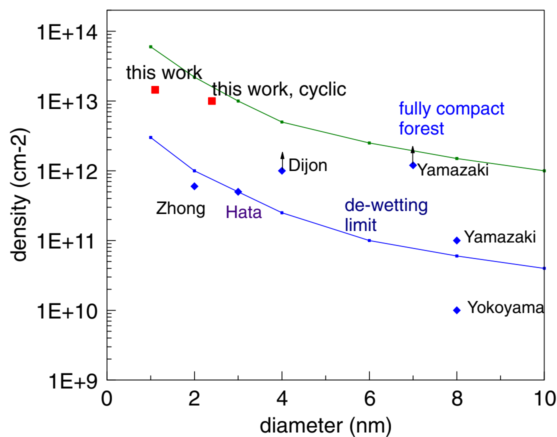

Fig. 10. (Color online) Nanotube densities achieved in this work, compared to previous works.[17,18,20,29,31,38] Wall densities are higher than tube densities for MWNTs.

catalyst into nanoparticles follows a fix set of trends from eqs. (12)–(14). This means that if we deposit one layer of catalyst, anneal it, then deposit a second layer and then anneal that, the second layer would merge with the first layer by sintering and give a particle diameter that was twice that from a single layer process, and a particle density N that was four times lower than from the single layer, rather than a higher density.

There is a way to overcome this limitation by depositing one layer, annealing it, then immobilising the particle layer,

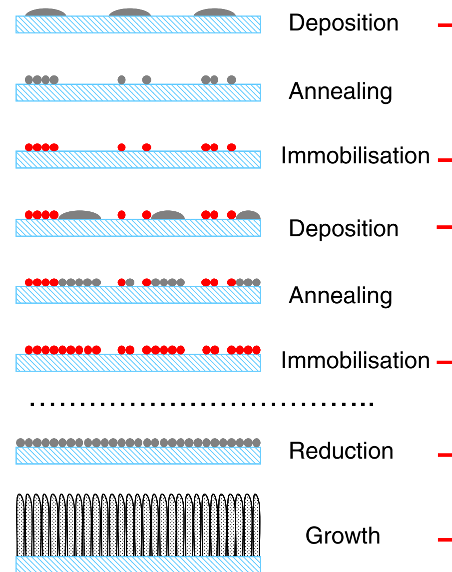

Fig. 11. (Color online) Schematic of the cyclic deposition process to produce higher density catalyst nano-particles.

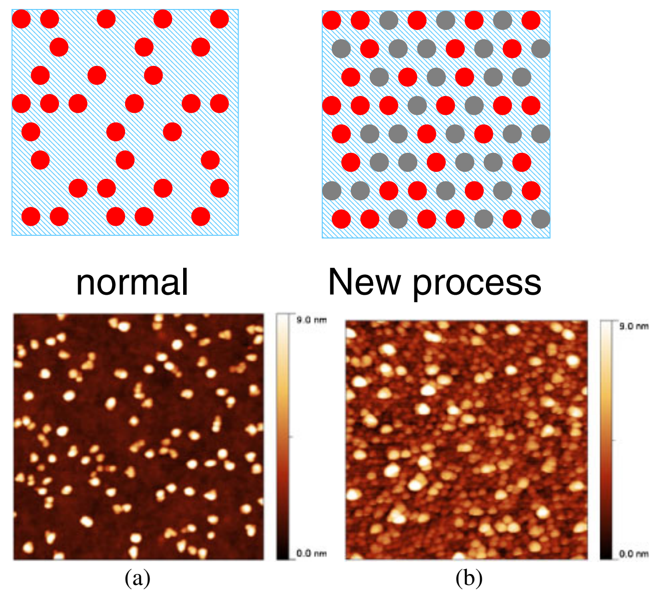

Fig. 12. (Color online) schematic of the catalyst nano-particles in (a) the normal catalyst process and (b) the cyclic deposition process, and below AFM images of the catalyst nano-particles.

then depositing another layer and annealing that. This time, the process is sequential, and the density will add cumulatively to a larger number, rather than reduce to a smaller number. Figure 11 shows the method in principle. Figure 12 shows an example of the method in practice, with atomic force microscope (AFM) images of the catalyst particles after one cycle and after two cycles. The experiment was done for a larger that normal film thickness so that the particles were more easily visible by AFM.

The catalyst is prepared using two cycles of 0.3 nm Fe onto Al_2O_3. Annealing is carried out in a tube furnace in Ar : H_2 = 1000 : 500 sccm atmosphere at 1 bar, from room temperature up to 750 °C at a heating rate of 75 °C min^{-1} for the first cycle and 25 °C min^{-1} for the second one. The

© 2012 The Japan Society of Applied Physics

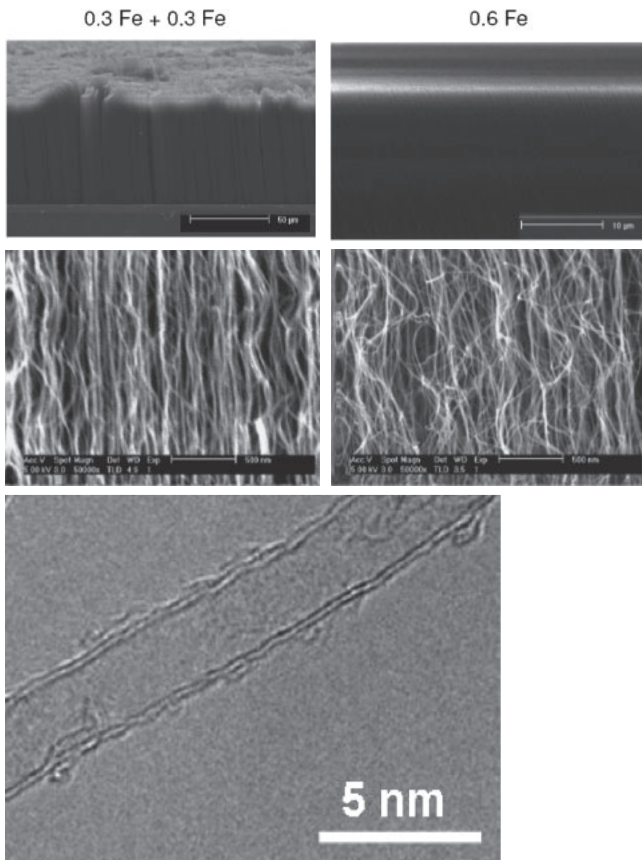

Fig. 13. SEM images of the nanotubes produced by (left) the cyclic catalyst process and (right) the normal process, and below a high resolution TEM image of the nanotubes.

sample is transferred in air between annealing steps. Fe depositions are performed at exactly same conditions. The CNTs were then grown in a furnace tube using Ar : H_2 : C_2H_2 = 1000 : 500 : 10 sccm for 15 min at 750 °C and 1 bar.

Figure 13(a) shows a high resolution cross sectional field emission gun scanning electron microscope (FEGSEM) image of our ultra-high density nanotube forest, where the tubes are so confined by adjacent tubes that they are much straighter than tubes in forests of previously typical density, such as Fig. 13(c). The high resolution TEM image in Fig. 13(b) shows that the nanotubes are mainly double walled, with mean diameter of 2.4 ± 0.2 nm. Raman finds a G/D peak ratio of over 6. The area density was estimated by the three methods as above, counting, weight gain and liquid induced compaction. Overall, a number of samples were grown with heights of 180–300 nm, CNT diameters of 2.2–2.6 nm, and mass density 0.911 to 1.03 g/cm^3, with the pitch between nanotube centres of 3.10 to 3.4 nm and resulting area densities of (0.92–1.10) $\times$ 10^{13} cm^{-2}. Figure 14 shows an SEM image of the forest before and after the liquid compaction.

The overall area density results are summarised in Fig. 10. We see that the cyclic density method gives a forest which starts to approach the ideal maximum dense forest. The density could be increase still further by making the diameter smaller. The small density result has a similar density, but is still quite far below the ideal maximum density.

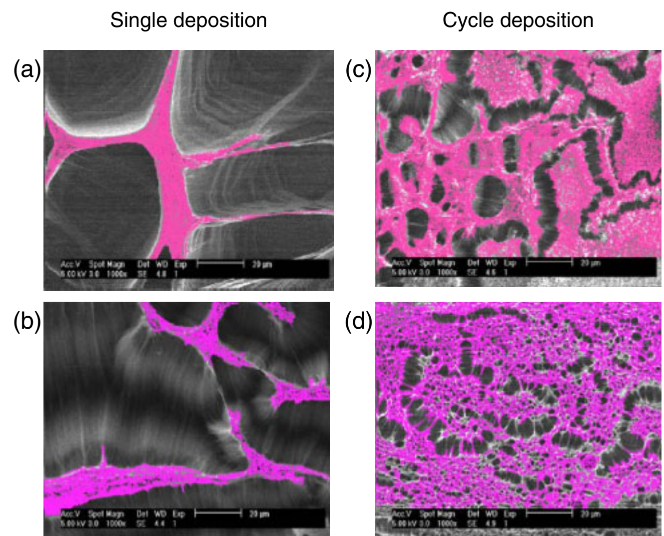

Fig. 14. (Color online) SEM image of liquid-induced compacted forest, for (a, b) single catalyst deposition process, and (c, d) cyclic deposition process.

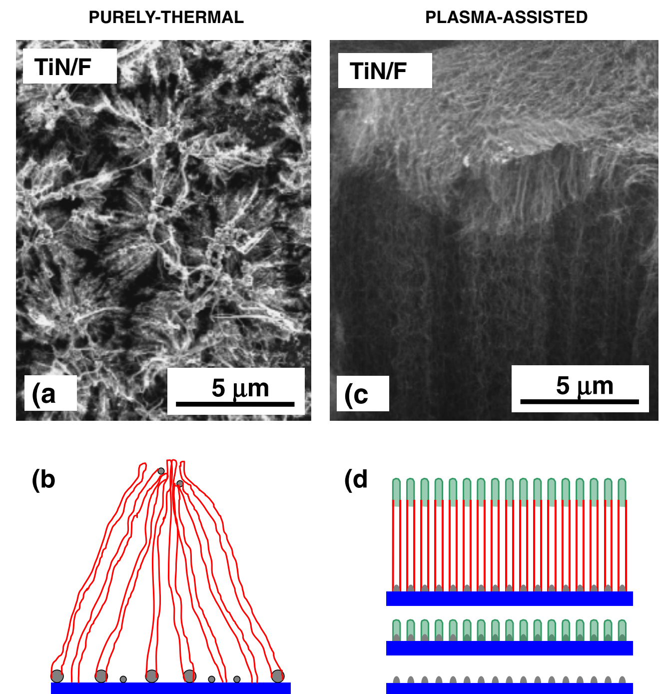

Fig. 15. (Color online) Showing how plasma pre-treatment of the catalyst enforces root growth. (a, b) No plasma. (c, d) Using plasma. Interrupted growth is used to show that a longer second growth step results in longer second step growth at the base or root.[68)]

It should be noted that for interconnect applications, the relevant value is the wall density, not tube density. The wall density is larger than the tube density for multiwalled nanotubes, as shown in Fig. 10.

There are other ways to increase nanotube density. First, it is necessary to ensure that the tubes grow by root growth.[68–71)] This can be checked by the interrupted growth method, as seen in Fig. 15.[68,72)] One way to enforce root growth is a plasma treatment step that increases the interfacial bonding of the catalyst to the support layer. It

© 2012 The Japan Society of Applied Physics

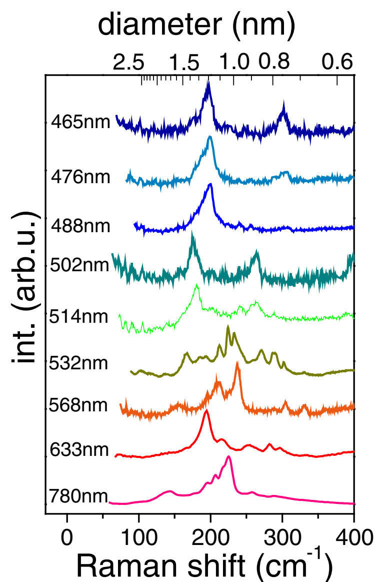

Fig. 16. (Color online) Raman spectra of high density forests at various excitation wavelengths.

also results in a narrower catalyst size distribution[73] and often a narrower average diameter. H_2, O_2, and N_2 plasmas are effective[20,68–71] and process gas optimisation.[37,74,75] A further way is to minimise sintering of the catalyst for example by a short carburisation step.[20]

4. Discussion

The vertically aligned forests have been characterised by Raman spectroscopy, in order to estimate the ratio of semiconducting to metallic nanotubes. The radial breathing mode (RBM) spectra are shown in Fig. 16. The modes are assigned using the usual relationship,[27] $\omega = C_1/D + C_2$ with $C_1 = 220.4 \pm 0.7$ and $C_2 = 7.4 \pm 0.7$. It is found that the chiralities have a random distribution. The chirality distribution is found to be random in terms of metallic to semiconducting ratio. It is true that some catalyst selection and/or treatment step can be used to enhance the metallic fraction.[76] However, there are higher priorities that this for growth for vias, such as density and low temperature growth. Whereas in a field effect transistor (FET), metallic nanotubes must be removed as they prevent the FET from being switched off, for interconnects semiconducting nanotubes are just dead space but otherwise they are not deleterious.

5. Process Integration

The nanotube growth process must then be made compatible with complementary metal oxide semiconductor (CMOS) fabrication processing. We are making considerable efforts to grow nanotubes on conducting substrates. There are two problems. First, metallic substrate have higher surfaces energies and thus inhibit the catalyst de-wetting process that forms the nano-particles. The second is that metals are reactive to oxygen and carbon, and can be converted into an insulating form. These processes are being studied by *in-situ* XPS and X-ray diffraction (XRD) to understand the preferred metal support.

A CMOS compatible growth process has been developed by Awano *et al.*[19] and Dijon *et al.*[29] In the Dijon process, the bottom contact is made of Al–Cu alloy, with 99% Al, a previous form of interconnect material. The process steps are as follows. The surface is first given a cleaning step to remove oxides and other potentially insulating layers. The catalyst is deposited and annealed to make the nano-particles. Dijon *et al.*[29,70] enforced root growth needed to ensure for high density mats by using an oxygen plasma treatment of the catalyst to increase the interfacial adhesion. Growth was carried out in a large area, low pressure CVD system. Growth continued until the nanotubes had emerged from the via holes. The holes around the nanotubes were then back-filled by Al_2O_3 by atomic layer deposition to provide mechanical integrity. The samples were then planarised by chemical mechanical polishing (CMP).[29] Then a top contact of Ti was applied, followed by a Pt overlayer. This is a similar set of steps as used by the Mirai group.[18,29]

It is still necessary to ensure that the process temperature is sufficiently low, 400 °C, which might be achieved by deposition in a remote plasma[19,38] as well as direct CVD.[40] It is useful to study the chemical state of the various layers by *in-situ* XPS during growth to ensure that the reactive metals do not accidentally form insulating layers.[69–71,77,78]

Acknowledgment

The authors acknowledge funding from the EC projects Viacarbon and Technotubes.

1) S. Frank, P. Poncharal, Z. L. Wang, and W. A. deHeer: Science **280** (1998) 1744.
2) Z. Yao, C. L. Kane, and C. Dekker: Phys. Rev. Lett. **84** (2000) 2941.
3) J. Kong, E. Yenilmez, T. W. Tombler, W. Kim, H. Dai, R. B. Laughlin, L. Liu, C. S. Jayanthi, and S. Y. Wu: Phys. Rev. Lett. **87** (2001) 106801.
4) J. Y. Park, S. Rosenblatt, Y. Yaish, V. Sazonova, H. Ustunel, S. Braig, T. A. Arias, P. W. Bronner, and P. L. McEuen: Nano Lett. **4** (2004) 517.
5) http://www.itrs.net/links/2009ITRS/2009Chapters_2009Tables/2009_Interconnect.pdf
6) A. Naeemi and J. D. Meindl: IEEE Electron Device Lett. **27** (2006) 338.
7) G. F. Close, S. Yasuda, B. Paul, S. Fujita, and H. S. P. Wong: Nano Lett. **8** (2008) 706.
8) B. Q. Wei, R. Vajtai, and P. M. Ajayan: Appl. Phys. Lett. **79** (2001) 1172.
9) J. Li and M. Meyyappan: Appl. Phys. Lett. **82** (2003) 2491.
10) M. Nihei, A. Kawabata, and Y. Awano: Jpn. J. Appl. Phys. **42** (2003) L721.
11) M. Nihei, M. Horibe, A. Kawabata, and Y. Awano: Jpn. J. Appl. Phys. **43** (2004) 1856.
12) M. Nihei, A. Kawabata, D. Kondo, M. Horibe, S. Sato, and Y. Awano: Jpn. J. Appl. Phys. **44** (2005) 1626.
13) D. Kondo, S. Sato, and Y. Awano: Chem. Phys. Lett. **422** (2006) 481.
14) M. Horibe, M. Nihei, D. Kondo, A. Kawabata, and Y. Awano: Jpn. J. Appl. Phys. **44** (2005) 5309.
15) Y. Awano, S. Sato, D. Kondo, and M. Neihi: Phys. Status Solidi A **203** (2006) 3611.
16) D. Yokoyama, T. Iwasaki, K. Ishimaru, S. Sato, T. Hyakushima, M. Nihei, Y. Awano, and H. Kawarada: Appl. Phys. Lett. **91** (2007) 263101.
17) D. Yokoyama, T. Iwasaki, K. Ishimaru, S. Sato, T. Hyakushima, M. Nihei, Y. Awano, and H. Kawarada: Jpn. J. Appl. Phys. **47** (2008) 1985.
18) Y. Yamazaki, N. Saluma, M. Katagiri, M. Suzuki, T. Sakai, S. Sato, M. Nihei, and Y. Awano: Appl. Phys. Express **3** (2010) 55002.
19) Y. Awano, S. Sato, M. Nihei, T. Sakai, Y. Ohno, and T. Mizutani: Proc. IEEE **98** (2010) 2015.
20) Y. Yamazaki: presented at Diamond Conf., 2010.
21) F. Kreupl, A. P. Graham, G. S. Duesberg, W. Steinhöegl, M. Liebau, E. Unger, and W. Hönlein: Microelectron. Eng. **64** (2002) 399.
22) F. Kreupl, A. P. Graham, M. Liebau, G. S. Duesberg, R. Seidel, and E. Unger: Electron. Dev. Meeting, IEDM Tech. Dig., 2004, p. 683.
23) A. P. Graham, G. S. Duesberg, R. Seidel, M. Liebau, E. Unger, F. Kreupl, and W. Honlein: Diamond Relat. Mater. **13** (2004) 1296.

 © 2012 The Japan Society of Applied Physics

24) G. D. Nessim, M. Seita, K. P. O'Brien, A. J. Hart, R. K. Bonaparte, R. R. Mitchell, and C. V. Thompson: Nano Lett. **9** (2009) 3398.
25) J. Robertson, G. Zhong, H. Telg, C. Thomsen, J. M. Warner, G. A. D. Briggs, U. Detlaff, S. Roth, and J. Dijon: Phys. Status Solidi B **245** (2008) 2303.
26) J. Robertson, G. Zhong, S. Hofmann, B. C. Bayer, C. S. Esconjauregui, H. Telg, and C. Thomsen: Diamond Relat. Mater. **18** (2009) 957.
27) J. Robertson, G. Zhong, S. Hofmann, B. C. Bayer, C. S. Esconjauregui, H. Telg, C. Thomsen, U. Detlaff, and S. Roth: Appl. Phys. Lett. **93** (2008) 163111.
28) J. Dijon, A. Fournier, P. D. Szkutnik, H. Okuno, C. Jayet, and M. Fayolle: Diamond Relat. Mater. **19** (2010) 382.
29) J. Dijon, H. Okuno, E. Quesnell, M. Fayolle, T. Vo, J. Pontcharra, D. Acquiviva, A. M. Ionescu, B. Capraro, C. S. Esconjauregui, and J. Robertson: Tech. Dig. IEDM, 2010, p. 32.6.
30) K. Hata, D. N. Futuba, K. Mizuno, T. Namai, M. Yumura, and S. Iijima: Science **306** (2004) 1362.
31) D. N. Futaba, K. Hata, T. Yamada, T. Hiraoka, Y. Hayamizu, Y. Kakudate, O. Tanaike, H. Hatori, M. Yumura, and S. Iiijima: Nat. Mater. **5** (2006) 987.
32) T. Yamada, T. Namai, K. Hata, D. N. Futaba, K. Mizuno, J. Fan, M. Yudasaka, M. Yumura, and S. Iijima: Nat. Nanotechnol. **1** (2007) 131.
33) Y. Murakami, S. Chiashi, Y. Miyauchi, M. H. Hu, M. Ogura, T. Okubo, and S. Maruyama: Chem. Phys. Lett. **385** (2004) 298.
34) Y. Miyauchi, S. Chiashi, Y. Murakami, Y. Hayashida, and S. Maruyama: Chem. Phys. Lett. **387** (2004) 198.
35) S. Noda, K. Hasegawa, H. Sugime, K. Kakehi, Z. Y. Zhang, S. Maruyama, and Y. Yamaguchi: Jpn. J. Appl. Phys. **46** (2007) L399.
36) K. Kakehi, S. Noda, S. Maruyama, and Y. Yamaguchi: Jpn. J. Appl. Phys. **47** (2008) 1961.
37) G. Zhong, T. Iwasaki, K. Honda, Y. Furukawa, I. Ohdomari, and H. Kawarada: Jpn. J. Appl. Phys. **44** (2005) 1558.
38) G. Zhong, T. Iwasaki, and H. Kawarada: Carbon **44** (2006) 2009.
39) G. Zhong, T. Iwasaki, J. Robertson, and H. Kawarada: J. Phys. Chem. B **111** (2007) 1907.
40) M. Cantoro, S. Hofmann, S. Pisana, V. Scardaci, A. Parvez, C. Ducati, A. C. Ferrari, A. M. Blackburn, K. Y. Wang, and J. Robertson: Nano Lett. **6** (2006) 1107.
41) S. Hofmann, R. Sharma, C. Ducati, G. Du, C. Mattevi, C. Cepek, M. Cantoro, S. Pisana, A. Parvez, F. Cervantes-Sodi, A. C. Ferrari, R. E. Dunin-Borkowski, and J. Robertson: Nano Lett. **7** (2007) 602.
42) S. Hofmann, M. Cantoro, B. Kleinsorge, C. Casiraghi, A. Parvez, J. Robertson, and C. Ducati: J. Appl. Phys. **98** (2005) 034308.
43) G. Zhong, S. Hofmann, F. Yan, H. Telg, J. H. Warner, D. Eder, C. Thomsen, W. I. Milne, and J. Robertson: J. Phys. Chem. C **113** (2009) 17321.
44) C. T. Wirth, C. Zhang, G. Zhong, S. Hofmann, and J. Robertson: ACS Nano **3** (2009) 3560.
45) S. S. Fan, M. G. Chapline, N. R. Franklin, T. W. Tombler, A. M. Cassell, and H. Dai: Science **283** (1999) 512.
46) A. J. Hart and A. H. Slocum: J. Phys. Chem. B **110** (2006) 8250.
47) Y. Q. Xu, R. E. Smalley, and R. H. Hauge: J. Am. Chem. Soc. **128** (2006) 6560.
48) P. B. Amama, C. L. Pint, S. M. Kim, L. McJilton, K. G. Eyink, E. A. Stach, R. H. Hauge, and B. Maruyama: ACS Nano **4** (2010) 895.
49) L. Zhang, Y. Q. Tan, and D. E. Resasco: Chem. Phys. Lett. **422** (2006) 198.
50) C. Mattevi, C. T. Wirth, S. Hofmann, R. Blume, M. Cantoro, C. Ducati, C. Cepek, A. Knop-Gericke, A. Goldoni, R. Schlogl, and J. Robertson: J. Phys. Chem. C **112** (2008) 12207.
51) R. Xiang, Z. Yang, Q. Zhang, G. Luo, W. Qiaun, F. Wei, M. Kadowaki, E. Einarsson, and S. Maruyama: J. Phys. Chem. C **112** (2008) 4892.
52) M. Pinault, V. Pichot, H. Khodja, P. Launois, C. Reynaud, and M. M. L'Hermitage: Nano Lett. **5** (2005) 2394.
53) G. Eres, A. A. Puretzky, D. B. Geohegan, and H. Cui: Appl. Phys. Lett. **84** (2004) 1759.
54) A. A. Puretzky, D. B. Geohegan, S. Jesse, I. N. Ivanov, and G. Eres: Appl. Phys. A **81** (2005) 223.
55) K. Hasegawa and S. Noda: ACS Nano **5** (2011) 975.
56) S. L. Kang, C. Kocabas, T. Ozel, M. Shim, N. Pimparkar, M. A. Alam, S. V. Rotkin, and J. A. Rogers: Nat. Nanotechnol. **2** (2007) 230.
57) H. Kataura, Y. Kjumazawa, Y. Maniwa, Y. Ohtsuka, R. Sen, and S. Suzuki: Carbon **38** (2000) 1691.
58) A. L. Giermann and C. V. Thompson: Appl. Phys. Lett. **86** (2005) 121903.
59) C. Zhang, F. Yan, C. S. Allen, B. C. Bayer, S. Hofmann, B. J. Hickey, D. Cott, G. Zhong, and J. Robertson: J. Appl. Phys. **108** (2010) 24311.
60) W. R. Tyson and W. A. Miller: Surf. Sci. **62** (1977) 267.
61) L. Vitos, A. V. Ruban, H. L. Skriver, and J. Kollár: Surf. Sci. **411** (1998) 186.
62) C. Sun and J. C. Berg: J. Chromatogr. A **969** (2002) 59.
63) R. K. Iler: *Chemistry of Silica* (Wiley, New York, 1998).
64) M. Marlo and V. Milman: Phys. Rev. B **62** (2000) 2899.
65) G. Eres, A. A. Kinkhabwata, H. T. Cui, D. B. Geohegan, A. A. Puretzky, and D. H. Lowdnes: J. Phys. Chem. B **109** (2005) 16684.
66) N. Chakrapani, B. Wei, A. Carrillo, P. M. Ajayan, and R. S. Kane: Proc. Natl. Acad. Sci. U.S.A. **101** (2004) 4009.
67) S. Esconjauregui, M. Fouquet, B. C. Bayer, C. Ducati, R. Smajda, S. Hofmann, and J. Robertson: ACS Nano **4** (2010) 7431.
68) S. Esconjauregui, B. C. Bayer, C. T. Wirth, S. Hofmann, and J. Robertson: Appl. Phys. Lett. **95** (2009) 173115.
69) C. S. Esconjauregui, M. Fouquet, B. C. Bayer, E. Eslava, S. Khachadorian, S. Hofmann, and J. Robertson: J. Appl. Phys. **109** (2011) 044303.
70) J. Dijon, P. D. Szkutnik, and A. Founrier: Carbon **48** (2010) 3953.
71) S. Esconjauregui, B. C. Bayer, M. Fouquet, C. T. Wirth, Y. Fan, R. Xie, C. Ductai, C. Baehtz, C. Castellarin-Cudia, S. Bhardwaj, C. Cepek, S. Hofmann, and J. Robertson: J. Appl. Phys. **109** (2011) 114312.
72) K. Liu, K. Jiang, C. Feng, Z. Chen, and S. S. Fan: Carbon **43** (2005) 2850.
73) C. Li, H. Zhu, K. Suenaga, J. Wei, K. Wang, and D. Wu: Mater. Lett. **63** (2009) 1366.
74) C. Zhang, C. T. Wirth, A. Parvez, C. Ducati, S. Hofmann, and J. Robertson: Diamond Relat. Mater. **17** (2008) 1447.
75) S. Pisana, A. Parvez, S. Hofmann, A. C. Ferrari, and J. Robertson: Physica E **37** (2007) 1.
76) A. R. Harutyunyan, G. Chen, T. M. Paronyan, E. M. Pigos, O. A. Kuznetsov, E. A. Stach, and G. U. Sumanasekera: Science **326** (2009) 116.
77) B. C. Bayer, S. Hofmann, C. Castellarin-Cudia, R. Blume, C. Baehtz, S. Esconjaurequi, C. T. Wirth, R. A. Oliver, C. Ducati, A. Knop-Gericke, R. Schlogl, A. Goldoni, C. Cepek, and J. Robertson: J. Phys. Chem. C **115** (2011) 4359.
78) B. C. Bayer, C. Zhang, R. Blume, F. Yan, M. Fouquet, C. T. Wirth, R. S. Weatherup, L. Lin, C. Baehrz, R. A. Oliver, A. Knop-Geriche, R. Schlogl, S. Hofmann, and J. Robertson: J. Appl. Phys. **109** (2011) 114314.

© 2012 The Japan Society of Applied Physics